Carrier kinetics and electron–polar-optical-phonon interaction in ZnSe studied by optically detected cyclotron resonance

Tatsuya Tomaru,* Tyuzi Ohyama, and Eizo Otsuka
Department of Physics, College of General Education, Osaka University, Toyonaka, Osaka 560, Japan

Minoru Isshiki
Research Institute of Mineral Dressing and Metallurgy, Tohoku University, Sendai 980, Japan

Kenzo Igaki†
Department of Materials Science, Faculty of Engineering, Tohoku University, Sendai 980, Japan
(Received 9 April 1992)

We have investigated the kinetics of photoexcited carriers in ZnSe by optically detected cyclotron resonance (ODCR). The results obtained are divided into two groups. The first is a group of phenomena originating in electron–polar-optical-phonon interaction: (1) resonant exciton formation following one LO-phonon emission; (2) resonance magnetic field of polaron cyclotron resonance is 4% higher in ODCR than in ordinary cyclotron resonance; (3) the formation rate of deep-acceptor-bound excitons is modulated by electron kinetic energy. The second is a group of phenomena related to two-dimensional (2D) electron systems constructed at a twin-boundary region: (1) magnetic field and its direction dependences of photoluminescence, ODCR, and thermally detected cyclotron resonance (TDCR), and (2) photoexcitation dependence of TDCR are observed, where one finds that the formation rate of bound states contributing to photoluminescence is dependent on the kinetic situation of the 2D electron system, and that I_3 and S lines in the photoluminescence spectrum are related to shallow impurities.

I. INTRODUCTION

Various attempts to grow single crystals of high-quality ZnSe have been made extensively for more than a decade, since ZnSe has been expected to work as an efficient blue-light-emitting device because of its proper band-gap energy of ~ 2.7 eV. Though this industrial purpose has not yet been realized, the appearance of high-quality samples has opened up a new place for physical study.

One of the physical investigations is the cyclotron-resonance study of electronic properties.[1–4] Through the cyclotron-resonance measurement, (1) electron effective mass, which reflects the structure of the conduction-band minimum, has been exactly determined;[1] (2) a polaron shift of cyclotron resonance has been observed;[2] and (3) heavy-hole cyclotron resonance has been observed.[3] In addition, the temperature dependence of the electron-scattering rate by electron-phonon and electron-neutral-impurity interactions was made clear through the linewidth measurements of cyclotron resonance.[2] Various crystal-growth methods of ZnSe have been attempted, e.g., vapor-phase epitaxy (VPE), liquid-phase epitaxy (LPE), and chemical vapor deposition (CVD). The VPE-grown crystal is generally of high quality. However, it is frequently twinned, causing some trouble in fabricating devices. The twin boundary, on the other hand, is a physically noticeable and appealing system, because it functions as a natural potential well for electrons. For this reason, some physical properties of the two-dimensional (2D) electron system constructed in this potential well have also been studied by cyclotron-resonance experiments.[2,4]

A detailed photoluminescence study of ZnSe was done by Merz *et al.*,[5] Dean *et al.*,[6] and Isshiki *et al.*[7] They succeeded in assigning most lines in the photoluminescence spectrum, especially shallow-donor-bound-exciton lines, by employing not only ordinary photoluminescence (PL) but also selective photoluminescence (SPL) and photoluminescence excitation (PLE) spectroscopy.

The aim of this paper is to study the electronic properties of high-quality ZnSe by optically detected cyclotron resonance (ODCR), which is a technique that combines cyclotron resonance (CR) and photoluminescence. We have so far extended ODCR in Ge and Si, where impact-dissociation processes of radiative objects, e.g., free excitons, bound excitons, or electron-hole droplets (EHD), by accelerated free carriers are key processes of the phenomena.[8–13] For ZnSe, there exists another additional aspect, namely, electron–polar-optical-phonon interaction. Thus we will discuss the effect of electron–polar-optical-phonon interaction in ODCR. The polaron concept will then play one key role. Next we will discuss the decay kinetics of photoexcited carriers by taking advantage of the fact that ODCR signals have information of both free carriers and excitonic systems. In our discussion, we will introduce a new technique that is somewhat similar to ODCR—thermally detected cyclotron resonance (TDCR).

II. EXPERIMENTAL PROCEDURE

Our experimental setup is composed of a Cd^+:He layer ($\lambda = 325$ nm, 25 mW) for photoexcitation, a 35-GHz-

microwave system for cyclotron resonance, and a photoluminescence-detecting system consisting of a spectrometer (Jasco Model No. CT-50) and a photomultiplier (Hamamatsu Model No. R980). It is more or less the same as the system described in Refs. 10 and 11, though the employed laser and detector are different. The microwave system is composed of a klystron (Oki Model No. 35V11), a nonresonant reflection-type waveguide system, and a diode detector (Alpha Model No. 1N26A). Photoluminescence and ordinary cyclotron-resonance absorption were measured using the excitation-light-modulation technique, while ODCR, i.e., change in photoluminescence due to cyclotron resonance, was measured by microwave modulation. The sample was set in a rectangular waveguide with Apiezon grease, where the microwave electric field was always perpendicular to the external magnetic field. The magnetic-field direction could be rotated in full 360° range. The waveguide holding the sample was enveloped in an airtight tube immersed in liquid helium. The airtight tube was filled with helium gas when the measurement was performed at 4.2 K, while it was made vacuous when the measurement was performed above 4.2 K. The temperature was monitored by a carbon resistor installed on the exterior face of the waveguide. The optical path for laser beam and luminescence was made of a silica rod (3 mm diam) in the cyrostat and a specially designed optical-fiber bundle divided into two paths, one of which was for the incident laser beam and the other for luminescence. For further details of the measuring system, see Refs. 10 and 11.

III. SAMPLES AND PHOTOLUMINESCENCE

The sample preparation is described in detail in Ref. 7. Polycrystalline ZnSe was first synthesized at 1000 °C and was refined by the sublimitation method. At the second stage, a single crystal was grown by vapor-phase transport using a Zn reservoir[14] at 1010 °C and a specially shaped growth chamber[15] at 1005 °C. This sample, which is so-called "as grown," has a number of Zn vacancies.[7] Zinc vacancies can be reduced with "Zn-dip" treatment.[7]

The samples used in the measurements were cut or cleaved from the grown single crystals. They all were nearly rectangular- or oval-shaped plates with maximum dimensions of $4\times3\times1$ mm^3. They were mechanically polished with No. 3000 emery paper and chemically etched at 90 °C for 2 min in a solution consisting of three parts saturated aqueous solution (at 60 °C) of $K_2Cr_2O_7$ and two parts concentrated H_2SO_4. The deposited selenium layer caused by the etching process was removed in CS_2.

All of the samples employed are n type, and their characteristics are listed in Table I. Their microscopic photographs, taken with a couple of optical polarizers, are shown in Fig. 1. The black stripes on samples 5 and 6 show twin boundaries. Twin boundaries give strong optical anisotropy; in other words, the dielectric-constant tensor of the twin-boundary region is different from that of the single-crystal region.

TABLE I. Sample characteristics. Sample numbers are the same as those in Ref. 2.

Sample	Treatment
4	As grown, without twin boundary
5	Zn dip
6	as grown

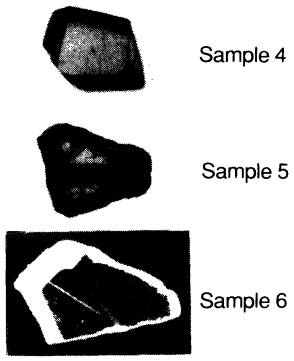

FIG. 1. Microscopic photographs of employed samples. Black stripes are twin boundaries. Photographed sample surface is a [110] crystallographic plane.

Schematic energy diagrams of the samples are shown in Fig. 2. Zinc vacancies V_{Zn}, which are numerous in as-grown samples, act as deep acceptors. The shallow donors in samples 4 and 6, therefore, are compensated. Sample 5, treated with the Zn-dip process, has few V_{Zn}, so that the shallow donors are not compensated, but a number of electrons have "fallen" into the potential wells of twin boundaries and exhibit 2D behavior in transport.[2,4] As for sample 6, the potential wells of twin boundaries have few electrons of the existence of V_{Zn}. Figure 3 shows a magnification of a potential-well part in sample 5. In the ground state, the electrons in the potential well exhibit 2D behavior, while they begin to exhibit three-dimensional (3D) behavior with an activation energy of 8.9 meV in the experiment of 35-GHz-microwave cyclotron resonance.[2] The 2D-to-3D transition in the experiment of cyclotron resonance occurs when the potential width exceeds the cyclotron diameter. The cyclotron radii of the lowest and next-lowest Landau levels are, respectively, $r\cong600$ and 1050 Å at $B=0.18$ T from the relation $[(2n+1)\hbar/eB]^{1/2}$, where n is the Landau quantum number.

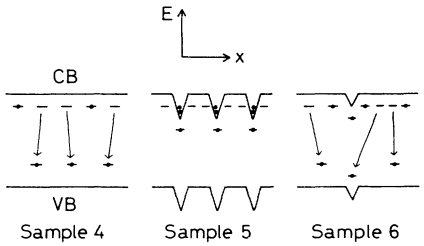

FIG. 2. Schematic energy diagrams of employed samples. Conduction band (CB), valence band (VB), shallow donor states, deep acceptor (V_{Zn}) states, and potential wells built in the twin-boundary region are drawn.

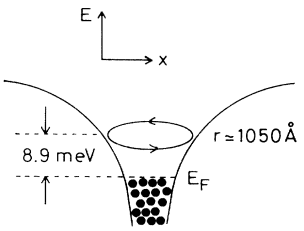

FIG. 3. Schematic image of the potential well at a twin boundary in sample 5. The work function is 8.9 meV for 35-GHz-microwave cyclotron resonance. Cyclotron radius r is about 1050 Å for the next-lowest Landau level.

Figure 4 shows the photoluminescence spectra of the three samples. The assignment of most lines on the spectra was done by the authors of Refs. 5, 6, 7, and 16; the I_1^d line is due to radiative recombination of excitons bound to deep acceptors[6] arising from Zn vacancies V_{Zn} and Cu impurities Cu_{Zn} of Zn sites.[7,16] For the employed samples, the I_1^d line due to Cu impurities is not observed; the I_1^d line is all due to Zn vacancies.[7] Radiative recombination of excitons bound to various neutral donors is labeled I_2 together, which is an ensemble of many lines and looks broadened, especially on sample 5. The radiative recombination lines labeled I_3 are controversial. They were first assigned to ionized-donor-bound excitons by Merz *et al.*,[5] while Isshiki *et al.*[7] judged this interpretation to be unreliable from the impurity-concentration dependence of I_2 and I_3 line intensities. We thus interpret I_3 lines as not due to ionized-donor-bound excitons. The assignment of the S line has not been done well, this problem will be mentioned in Sec. IV C.

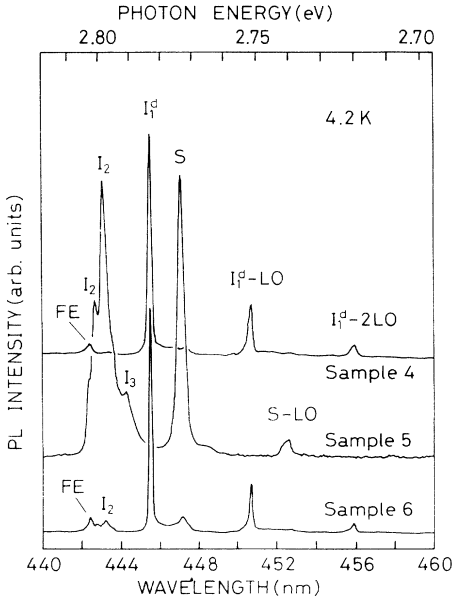

FIG. 4. Photoluminescence spectra of employed samples.

IV. DECAY KINETICS

A. Hypothesis on the decay processes

In this section we describe the basic order of the carrier-decay processes, which will be employed as a fundamental principle of the analysis of the experimental results in Sec. IV B. The carrier-decay processes are often accomplished through phonon emissions. Here the optical phonon, whose energy is sufficiently larger than the thermal energy of free carriers at ~ 10 K and whose absorption by free carriers therefore is rare, is especially important for decay processes; in addition, among optical phonons the LO phonon is most important, because it is polar and therefore exhibits a strong carrier-phonon interaction through the induced electric field. It is thus expected that the carrier-decay processes are dominated by LO phonon emissions.

Decay processes of carriers photoexcited into the high-energy states of the bands are constructed by the following processes: first, photoexcited carriers relax to the band edge; next, they are captured by some traps to fall into bound states; and, finally, the electron-hole pairs recombine. In this paper we deal mainly with the second process. The capture rate, at which free carriers are captured into some bound state, is generally given by

$$1/\tau = N v(E) \sigma(E) , \tag{1}$$

where N, v, E, and σ are the trap concentration, free-carrier velocity, kinetic energy of free carriers, and capture cross section of the traps, respectively. The dependence of $\sigma(E)$ on E can be roughly understood from the following two classification schemes.

(1) The first is when $\varepsilon_b \gtrsim \hbar\omega_{LO}$, where ε_b and $\hbar\omega_{LO}$ are the binding energy of a bound state and the LO-phonon energy, respectively. Then a free carrier can be captured into a bound state by emitting an LO phonon, and the bound carrier cannot be released to the conduction or valence band at ~ 10 K because $\hbar\omega_{LO} \gg k_B T$ and the number of thermally excited LO phonons is very small. Thus free carriers are always captured when impinging on traps unless $E > \hbar\omega_{LO}$; if $E > \hbar\omega_{LO}$, the free carrier remains in a conductive state even after one LO-phonon emission. It is expected, according to the above situation, that $\sigma(E)$ just weakly depends on E unless $E > \hbar\omega_{LO}$. The capture rate τ^{-1} will increase linearly with v and be modulated by $\sigma(E)$.

(2) The second is when $\varepsilon_b < \hbar\omega_{LO}$. Then a free carrier cannot emit an LO phonon at capture unless $\epsilon_b + E > \hbar\omega_{LO}$. Only acoustical phonons can be emitted. Since the energy of the particular acoustical phonons taking part in the carrier-decay processes through the deformation-potential interaction is $\sim k_B T$, there are very few possibilities that a free carrier with $E > \sim k_B T$ is captured with only one acoustical-phonon emission. A capture process is not achieved unless multiple phonons are emitted, which is a higher-order process. Thus, $\sigma(E)$ will be a monotonically decreasing function of E. The situation is changed, however, when $E + \varepsilon_b > \hbar\omega_0$. Then the free carrier can emit one LO phonon,[17] and therefore $\sigma(E)$ suddenly grows. This tendency is also familiar for

the capture rate, though a factor of v is added.

We can now say that the characteristic decay process is determined from comparison of a physical quantity with the LO-phonon energy. In Sec. IV B we analyze the experimental results according to the above consideration.

B. Sample 4: ODCR of a polaron

The existence of a twin boundary necessarily has an influence on carrier kinetics. Here we show the experimental results in sample 4, which is not twinned. They will make the behavior of carriers in single-crystal ZnSe clear, where strong electron–polar-optical-phonon interaction turns up in a principal role. The twin boundary, which forms a natural potential well, will be dealt with in Secs. IV C and IV D.

Figure 5 shows an ordinary cyclotron-resonance trace and ODCR traces for sample 4 which are expressed with changes in photoluminescence intensities of the free-exciton line (FE). The relative microwave power is indicated on the right. The ordinary cyclotron-resonance trace is constructed with a nonresonant background and electron cyclotron-resonance absorption. The former is probably due to carrier absorption in a low-mobility region near the band edge originating in some stacking fault, because the ratio of the background intensity to the electron cyclotron-resonance absorption intensity decreases with an increase in microwave power corresponding to electron kinetic energy. The peak position of ordinary cyclotron resonance varies to the high field side by about 1% as microwave power increases to the maximum. Each ODCR trace, roughly speaking, shows a decrease in luminescence intensity with increasing microwave power, which is due to a decrease in the free-exciton-formation rate caused by increasing electron kinetic energy, where the binding energy of free excitons is $\varepsilon_x \cong 20$ meV (Ref. 18) and $\hbar\omega_{\mathrm{LO}}$ is 31.8 meV (see Fig. 6). However, there is a peak which strongly depends on microwave power at a magnetic field 4% higher than the peak position of ordinary cyclotron resonance obtained with -10-dB microwaves. Considering the strong dependence of this peak on microwave power, we expect it is caused by a resonant formation of free excitons. According to the hypothesis in Sec. IV A, the resonant formation occurs at

$$E=\hbar\omega_{\mathrm{LO}}-\varepsilon_x \cong 11.8 \text{ meV} ,$$

following one LO-phonon emission (see Fig. 6). Then, why is the peak position of ODCR 4% higher, though the variation of the peak position of ordinary cyclotron resonance is only about 1% within the possible microwave power? One possibility is a polaron effect. The ordinary cyclotron-resonance line is a sum of absorption by all phonon-dressed conduction electrons, i.e., by all polarons, while the peak of the ODCR trace for high microwave power is caused only by the polarons which are heated up to more than 11.8 meV through cyclotron-resonance absorption. Hence we try to estimate the effective-mass shift caused by a polaron effect.

First, we deal with the weak-coupling case ($\alpha \ll 1$). The energy dispersion of polarons at $T=0$ K is given by[19]

$$E=-\alpha\hbar\omega_{\mathrm{LO}}+\frac{\hbar^2k^2}{2m_b}\left[1-\frac{\alpha}{6}\right]-\frac{3}{160}\frac{\hbar^3\alpha k^4}{m_b^2\omega_{\mathrm{LO}}} , \quad (2)$$

where the higher-order terms with respect to k are neglected and α is the dimensionless coupling constant

$$\alpha=\frac{e^2}{\hbar}\left[\frac{1}{\varepsilon_\infty}-\frac{1}{\varepsilon_0}\right]\left[\frac{m_b}{2\hbar\omega_{\mathrm{LO}}}\right]^{1/2} ; \quad (3)$$

m_b, ε_∞, and ε_0 are the bare electron effective mass and the optical and the static dielectric constants of the host lattice, respectively. Using the Bohr-Sommerfeld quantization rule, Bajaj derived the cyclotron effective mass $m_\perp$ of polarons from Eq. (2):

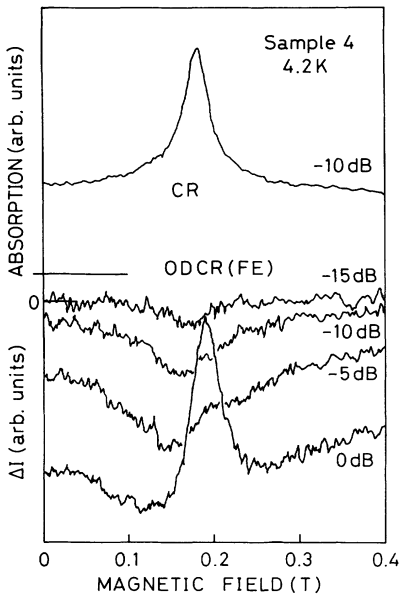

FIG. 5. ODCR traces obtained from observation of the FE line in the photoluminescence spectrum and ordinary cyclotron-resonance trace. The ODCR traces show the changes in luminescence intensity due to cyclotron resonance. The downward deviation means the decrease in luminescence intensity. Values indicated in decibels are relative microwave powers.

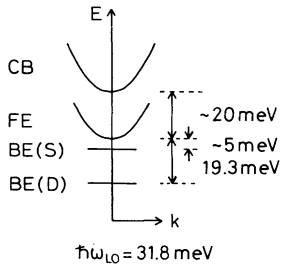

FIG. 6. Schematic energy diagram of various exciton states. Free-exciton (FE), shallow-donor-bound excition [BE(S)], and deep-acceptor (V_{Zn}) -bound exciton [BE(D)] states are drawn.

$$\frac{m_b}{m_\perp}=1-\frac{\alpha}{6}-\frac{3}{20}\alpha\left[\hbar\omega_c\left(n+\tfrac{1}{2}+\gamma\right)+\frac{\hbar^2k_z^2}{2m_b}\right]\Big/\hbar\omega_{\mathrm{LO}}\ , \tag{4}$$

where $\omega_c=eB/m_b$, $0\le\gamma\le1$, and n is the Landau quantum number. Approximating Eq. (4) to a classical representation, we get

$$\frac{m_b}{m_\perp}=1-\frac{\alpha}{6}-\frac{3}{20}\alpha\frac{\hbar^2k^2}{2m_b}\Big/\hbar\omega_{\mathrm{LO}}\ . \tag{5}$$

We will now estimate the effective-mass shift from Eq. (5). The coupling constant α may be estimated from ε_∞ and ε_0 according to Eq. (3). However, reported values of ε_∞ and ε_0 vary as widely as about 20%,[20] so that the exact value of α has not been determined. In this situation, Ohyama *et al.*[2] determined $\alpha=0.575$ from the formula by Peeters and Devreese[21] and an experiment of polaron cyclotron resonance in a far-infrared region. We thus use $\alpha=0.575$. Then,

$$m_\perp(\hbar^2k^2/2m_b=12\ \mathrm{meV})/m_\perp(0\ \mathrm{meV})\cong1.037$$

from Eq. (5), that is, the mass shift is 3.7%.

The formulation is also similar for the intermediate-coupling case[22] ($\alpha\lesssim6$);

$$E=-\alpha\hbar\omega_{\mathrm{LO}}+\frac{\hbar^2K^2}{2m_b}\left[1+\frac{\alpha}{6}\right]^{-1}-\frac{3}{160}\frac{\hbar^3\alpha K^4}{m_b^2\omega_{\mathrm{LO}}}\left[1+\frac{\alpha}{6}\right]^{-4}, \tag{6}$$

$$\frac{m_b}{m_\perp}=\left[1+\frac{\alpha}{6}\right]^{-1}-\frac{3}{20}\alpha\frac{\hbar^2K^2}{2m_b}\left[1+\frac{\alpha}{6}\right]^{-4}\Big/\hbar\omega_{\mathrm{LO}}\ , \tag{7}$$

where K is the sum of wave vectors of an electron and phonons constructing a polaron. From Eq. (7), the mass shift is estimated at 2.5% or

$$m_\perp(\hbar^2k^2/2m_b=12\ \mathrm{meV})/m_\perp(0\ \mathrm{meV})\cong1.037$$

Judging from the above estimations, we may say that the peak shift of 4% between the ordinary cyclotron resonance and the ODCR is caused by the polaron effect. The reason the variation of the peak position of ordinary cyclotron resonance is only about 1% within the possible microwave power is that the signal of the ordinary cyclotron resonance consists of the resonances of both low- and high-energy polarons.

Now let us turn our attention to ODCR signals shown in Fig. 7 obtained from the observation of excitons bound to deep acceptors V_{Zn} (the I_1^d line in the photoluminescence spectrum). Each ODCR trace, roughly speaking, shows an increase in luminescence intensity with an influence of cyclotron resonance. To understand this phenomenon, we discuss the formation process of excitons bound to deep acceptors V_{Zn}. Three kinds of formation processes should be considered. The first is the case when the deep acceptors capture free excitons:

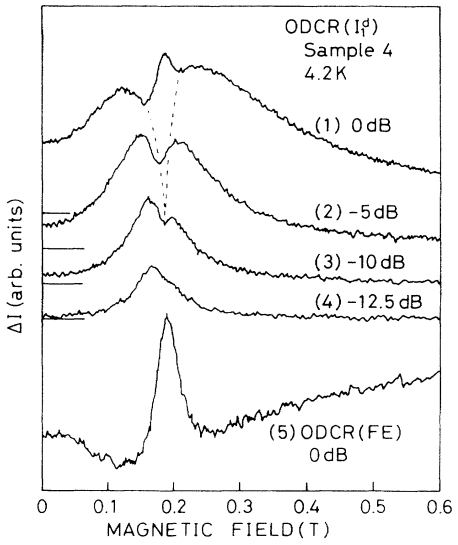

FIG. 7. ODCR traces obtained from the I_1^d line with various microwave powers [(1)–(4)]. For comparison, an ODCR trace (5) obtained from the FE line is added, which is the same as the trace labeled 0 dB in Fig. 5.

$$A^0+e^-+h^+\rightarrow A^0+X\rightarrow(A^0,X)\ ,$$

where A^0, e^-, h^+, X and (A^0,X) are a neutral acceptor, an electron, a hole, a free exciton, and an acceptor-bound exciton, respectively. The second is the case when electrons are captured after holes are captured by neutral acceptors:

$$A^0+h^++e^-\rightarrow A^++e^-\rightarrow(A^0,X)\ .$$

The third is the case when holes are captured after electrons are captured by neutral acceptors:

$$A^0+e^-+h^+\rightarrow(A^-,X)+h^+\rightarrow(A^0,X)\ .$$

We can neglect the last case because the (A^-,X) state has not been observed so far. Then which is a dominant process, the first or the second case? If the first is dominant, the formation process is sharply resonant with electron kinetic energy and strongly depends on microwave power because the free-exciton-formation process is so (see Fig. 5). Experimental results in Fig. 7, however, show broad resonance lines as a base. We thus conclude that the second is the dominant process. Then, why does the luminescence intensity of the I_1^d line increase with microwave power? This is probably because the binding energy for an electron in one (A^0,X) state is nearly equal to or more than $\hbar\omega_{\mathrm{LO}}$, that is, the situation is applicable to the case of $\varepsilon_b\gtrsim\hbar\omega_{\mathrm{LO}}$ in Sec. IV A. In this case, the electron-capture rate by A^+ centers increases with electron velocity v according to Eq. (1). The reason the peak position on trace (4), which has no fine structure, is at a magnetic field lower than that on trace (5) is probably because the electron-capture rate τ^{-1} by A^+ centers comes to a maximum at a relatively low kinetic energy of electrons. We can thus understand ODCR traces in Fig. 7 on the whole. Then, what is the fine

structure on each trace? We expect it is due to electron-energy dependence of capture cross section $\sigma(E)$; in other words, the capture rate is basically determined by v and modulated by $\sigma(E)$.

Since bound excitons have no freedom of translation, their energy levels are completely discrete. Accordingly, the formation process of bound excitons can be accomplished only when the condition

$$\varepsilon_{b\alpha}+E=n\hbar\omega_{\mathrm{LO}} \tag{8}$$

is satisfied, where α indexes an energy level in the bound states and n is an integer. Thus, $\sigma(E)$ should strongly depend on free-carrier kinetic energy E. This tendency is especially high for deep-impurity-bound excitons, because the space between discrete levels is rather wide. By considering the condition of Eq. (8), we try to intrepret the fine structures on ODCR traces in Fig. 7.

First, we assume that the condition of Eq. (8) is nearly satisfied in the electron-capture process by A^+ centers under a thermal equilibrium of 4.2 K. Then the capture rate τ^{-1} increases with electron velocity v according to Eq. (1). As shown by traces (1)–(4) in Fig. 7, the luminescence intensity reflecting τ^{-1} first increases as electrons are heated through the cyclotron-resonance absorption. However, when electrons are "overheated," Eq. (8) will no longer be satisfied. The dip on trace (3) could be attributed to that fact. On trace (4), also, the interpretation is applicable, where the dip on the trace disappears due to low microwave power. As for traces (1) and (2), the situation is complicated. On trace (2), the dip position is shifted to the left side, compared with that on trace (3), and trace (2) is raised up at the magnetic field where trace (3) exhibits the dip. This situation is more extreme on trace (1).

An interpretation is simple. The higher the microwave power becomes, the larger the dip size becomes, while a new peak begins to emerge at the magnetic-field position where trace (5) exhibits a peak. The left shift of the dip position on trace (2) should thus be interpreted not as a real shift but as an apparent one. If so, what does the new peak originate in? Here are two interpretations.

The first is an effect of a higher-energy polaron. The reason for a dip on each trace is based on the fact that Eq. (8) is no longer satisfied for the ground state of the bound states when electrons are overheated. If so, it is expected that Eq. (8) may be satisfied for an excited state of the bound states if electrons are still more heated. The effective mass given by the new-peak position in such a case should be heavier owing to the polaron effect than that given by the dip position of trace (3). The new peak, however, emerges at almost the same magnetic field as trace (3) exhibiting the dip. Accordingly, the first possibility is ruled out.

The second interpretation is an effect brought about from resonant formation of free excitons. As mentioned before, the dominant formation process of excitons bound to V_{Zn} is electron capture by A^+ centers. However, neutral acceptors can also capture free excitons. As shown in Fig. 5, free excitons are resonantly formed with 0-dB microwaves. Similarly, the new peak in Fig. 7 becomes clear with 0-dB microwaves, and the peak position coincides with the magnetic field at which free excitons are resonantly formed. We thus expect that the new peak in Fig. 7 is brought from the process where neutral acceptors capture free excitons. From the discussion in this section, we can conclude that carrier kinetics in ZnSe is determined by strong electron–polar-optical-phonon interaction.

C. Sample 5

Since the region of the twin boundary acts as a potential well for electrons, photoexcited electrons should promptly fall into these wells. We discuss here the influence of the potential wells upon the decay kinetics of photoexcited carriers on the stage of sample 5, which accumulates electrons in the potential wells even without photoexcitation owing to Zn-dip treatment.

Figure 8 shows ODCR traces obtained from various lines in the photoluminescence spectrum. Qualitatively each trace behaves in the same way. Besides, the line shape of each trace is almost independent of microwave power. This situation suggests that the bound states giving I_2, I_3, and S lines are not related to deep impurities or free excitons and that their formation processes are not related to the free-exciton state. This is because the ODCR traces obtained in sample 4 are related to deep impurities and free excitons, and they are strongly dependent on microwave power.

Figure 9 shows a dependence of the ODCR trace on magnetic-field direction, which is obtained from observation of the S line. The ODCR traces obtained from I_2 and I_3 lines also have the same dependence on magnetic-field direction. The dependence demonstrates the nature of the 2D system, because the effective magnetic field determining the phenomenon is the magnetic-field component perpendicular to the plane of twin boundaries.[2,4] As shown in Fig. 9, only cyclotron resonance of the 2D system is observed, while that of bulk electrons which have three degrees of freedom and an isotropic nature is

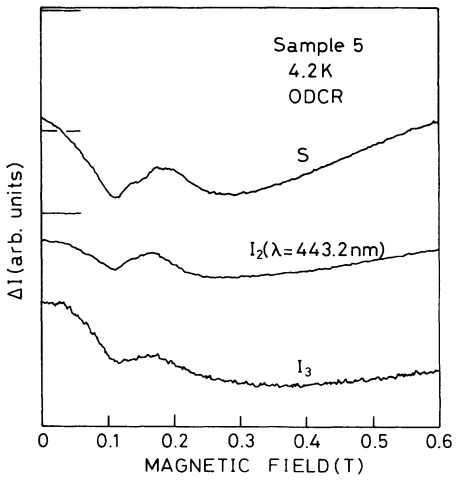

FIG. 8. ODCR traces obtained from various luminescence lines. The magnetic-field direction is perpendicular to the plane of twin boundaries. The relative microwave power is −5 dB.

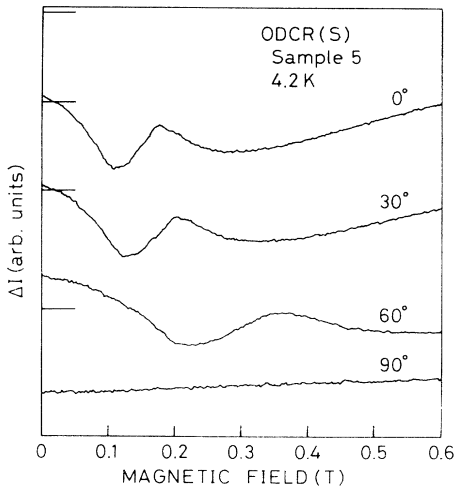

FIG. 9. Angular dependence of ODCR trace obtained from the S line. The angles shown are those between magnetic-field direction and the normal to the twin boundary plane. The relative microwave power is -5 dB.

not observed. This means that the photoexcited electrons have immediately fallen into the potential wells which construct the 2D system. If bulk electrons exist in abundance, a resonance line independent of magnetic-field direction should appear.[2,4]

Figure 10(a) shows the magnetic-field dependence of various luminescence lines obtained without microwaves. Every line shows the largest decrease in luminescence intensity when the magnetic field is perpendicular to the plane of twin boundaries. This, similar to Fig. 9, reflects the 2D nature. On sample 4, which is not twinned, the dependence of the luminescence intensity upon magnetic-field direction has never been observed. The similarity in Fig. 10(a) between three luminescence lines about magnetic-field dependence should be noted together with that in Fig. 8. In Fig. 11 the photoluminescence spectra under the magnetic fields of 0 and 0.6 T are shown. No change in line shape of the photoluminescence spectrum is found, so that the effect of magnetic field is a simple reduction of luminescence intensity.

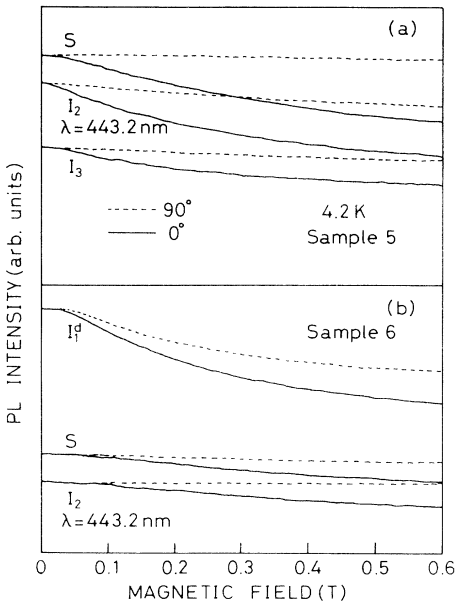

FIG. 10. Magnetic-field dependence of luminescence intensities of various lines. Solid and dashed traces are drawn, respectively, with the magnetic field perpendicular and parallel to the plane of twin boundaries. The scale of the vertical axis is different for each trace. The magnetic-field dependence obtained with other field directions is between the solid and dashed traces.

Here we briefly mention the assignment of the luminescence lines. As mentioned in Sec. III, the I_2 line is an ensemble of radiative-recombination lines of excitons bound to various neutral donors, while the I_3 line was first assigned to radiative recombination of ionized-donor-bound excitons. The I_3 assignment, however, is controversial now.[7] We cannot determine here the origin of the I_3 line. But we might say that it is at least related to shallow impurities, judging from similarity between I_2 and I_3 lines in Figs. 8 and 10(a) as well as the correlation between I_2 and I_3 lines described in Ref. 7. As to the S line, Merz *et al.*[5] proposed that it was an LA-phonon replica of the I_1^d line. However, we expect it to be related to shallow impurities, judging from Figs. 8 and 10(a). This expectation is supported by Figs. 12 and 10(b), showing experimental results on sample 6. Figure 12 shows a change in the photoluminescence spectrum induced by cyclotron resonance near resonance magnetic field, where I_2 lines as well as the S line and its replica are directed downward, while the I_1^d line and its replicas related to deep impurities are directed upward. Figure 10(b) shows the magnetic-field dependence of luminescence intensities. Even when the magnetic-field direction is parallel to the plane of twin boundaries, the I_1^d line is dependent on magnetic-field strength, while the I_2 and S lines have almost no dependence. Thus, the S line is expected to be related to shallow impurities. However, the S line is not

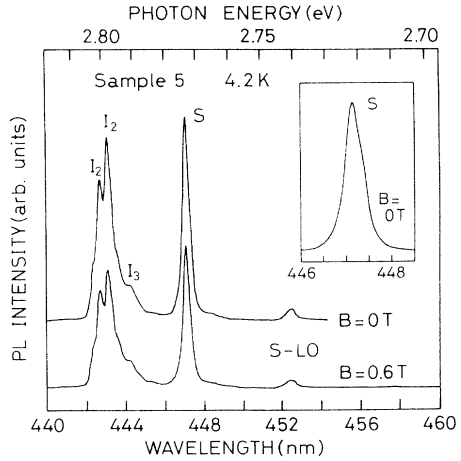

FIG. 11. Magnetic-field dependence of photoluminescence spectrum. The magnetic-field direction is perpendicular to the plane of twin boundaries. The inset is a magnification of the S line at 0 T. The right side of the peak is swollen.

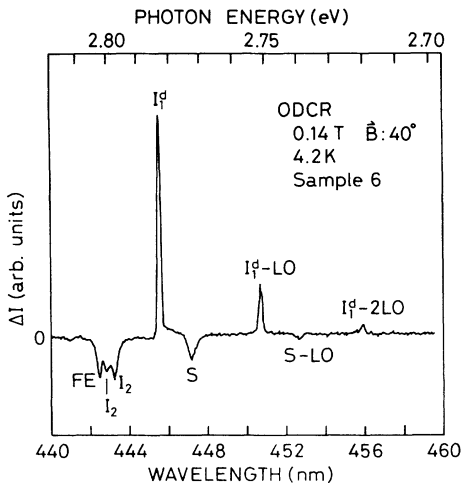

FIG. 12. Change in photoluminescence spectrum induced by cyclotron resonance. The relative microwave power is 0 dB. The angle of the magnetic field is measured the same in Fig. 9.

so simple. It appears from two origins at least, as shown in the magnification in Fig. 11. We are thus unable to make an exact assignment of the *S* line. One thing we can say is that the *S* line is related to shallow impurities. For more exact assignment, further detailed studies are needed.

We now discuss the magnetic-field dependence of the luminescence intensity. As shown in Fig. 10(a), the intensity of each luminescence line is almost independent of the magnetic-field strength when the magnetic field is parallel to the plane of twin boundaries, while it varies most widely when the magnetic field is perpendicular to the plane of twin boundaries. This indicates that photoluminescence is related to the potential wells and that effective magnetic field determining the luminescence intensity is the magnetic-field component perpendicular to the plane of twin boundaries. Hence we discuss a relationship between the photoluminescence and the potential wells mainly by noting the case in which magnetic-field direction is perpendicular to the plane of twin boundaries. There are two interpretations as to the magnetic-field dependence of the luminescence intensity. The first is that the formation rate of bound states contributing to photoluminescence depends on magnetic field. The second is that the radiative efficiency depends on magnetic field. In the first interpretation, the decrease in luminescence intensity with increasing magnetic field in Fig. 10(a) means that photoexcited electrons stay longer in the potential wells under high magnetic field than under low magnetic field before being captured into the bound states. In the second interpretation, the bound states contributing to photoluminescence must be formed in the potential wells, because the magnetic-field dependence of photoluminescence reflects the anisotropy of the potential-well structure.

Which of the two interpretations is correct? This question is answered from consideration of Fig. 13. Figure 13 shows thermally detected cyclotron resonance. It is a technique by which we detect an increase in sample temperature due to cyclotron resonance; the increase in sample temperature is a result of the fact that free carriers heated up through cyclotron-resonance absorption emit phonons in their relaxation process. To our knowledge, our observation is the first report on TDCR. In sample 5, a number of electrons exist in the potential wells even without photoexcitation on account of Zn-dip treatment, so that TDCR is observed even without photoexcitation as shown in Fig. 13(a). The dependence of TDCR upon magnetic-field direction again reflects the nature of the 2D electron system, similar to ODCR in Fig. 9. Figure 13(b) shows TDCR with photoexcitation. Dependence on magnetic-field direction is the same as that of Fig. 13(a). In Fig. 13(b), cyclotron resonance of bulk electrons is not found, which is similar to Fig. 9 and suggests that photoexcited electrons have immediately fallen into the potential wells. A clear difference between Figs. 13(a) and 13(b) is the behavior on the high magnetic-field side of the electron cyclotron-resonance line. If photoexcited electrons contribute to TDCR in the same manner as electrons naturally located in the potential wells, the line shape of TDCR should be the same between Figs. 13(a) and 13(b). However, Fig. 13 demonstrates that photoexcited electrons contribute to TDCR greater at high magnetic field than at low magnetic field, which suggests that the number of photoexcited electrons staying in the potential wells is larger at the higher-magnetic-field side. This can be understood if the first interpretation of the luminescence intensity on magnetic-field dependence is adopted, because a decrease in luminescence intensity with increasing magnetic field in Fig. 10(a) means that photoexcited electrons stay longer in the potential wells under high magnetic field than under low magnetic field before being captured into the bound states. We have thus proved that the formation rate of the bound states contributing to photoluminescence is a function of magnetic field and is determined by the magnetic-field component perpendicular to the plane of twin boundaries. The fact that the perpendicular component of magnetic

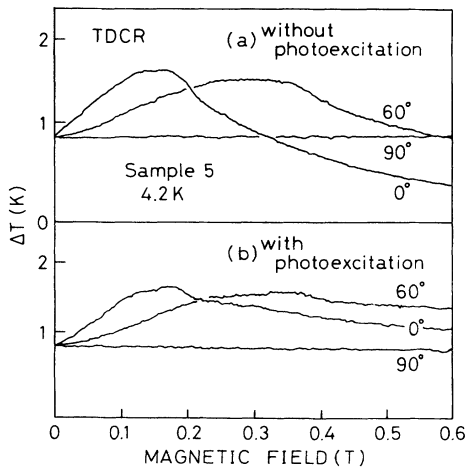

FIG. 13. TDCR traces obtained with 0-dB microwaves. The vertical axis shows the temperature increase measured with a thermometer. A temperature increase due to photoexcitation is excluded. Angles are defined as in Fig. 9.

field determines the phenomenon suggests that the formation rate of the bound states is dependent on the kinetic situation of the 2D electrons influenced by the magnetic field.

Finally, we get back to the subject of ODCR. Every ODCR trace in Fig. 8 shows a decrease in luminescence intensity with an influence of cyclotron resonance though some structure is observed. This result corresponds to the second case in Sec. IV A. This correspondence is just natural, since luminescence lines labeled I_2, I_3, and S are all expected to be related to shallow impurities. One problem is a particular structure near resonance magnetic field in Fig. 8. This structure is observed, independent of microwave power, so that it has no relationship to resonant formation of free excitons or resonant emission of LO phonons. One possibility is that it may be related to a nature of the potential wells. No decisive evidence is yet available, however. This question, together with that of the magnetic-field dependence of photoluminescence, should be studied further.

D. Sample 6

Since sample 6 possesses both V_{Zn} and twin boundaries, the kinetics of photoexcited carriers reflects both characteristics of samples 4 and 5. A difference from sample 5 is that the potential well, built at the twin-boundary region, does not accommodate electrons on account of the existence of V_{Zn} and that the potential well is not so deep as that of sample 5. Because of the second difference, cyclotron resonance of bulk electrons is observed in sample 6 with photoexcitation and that of the 2D electron system is not; in sample 5, only cyclotron resonance of the 2D system is observed and that of bulk electrons is not, even with photoexcitation. The difference in the potential-well nature between samples 5 and 6 appears in TDCR also. The reason TDCR is observed in sample 5 is that sample 5 has no V_{Zn}, which act as acceptors for donor compensation, and accumulates a number of electrons in the potential wells. For this reason, TDCR is not observed in samples 4 and 6, because they possess V_{Zn} and therefore cannot call enough free carriers into existence even with photoexcitation.

With these remarks, we show experimental results on sample 6. Figure 10(b) shows magnetic-field dependence of each luminescence line; photoluminescence of sample 6 is shown in Fig. 4. Owing to the existence of twin boundaries, there is a dependence on magnetic-field direction. As for sample 4, which is not twinned, the dependence on magnetic-field direction has not been observed. An influence of twin boundaries appears in ODCR also. Figure 14 shows ODCR traces obtained from the I_1^d line. The general behavior is the same as that in Fig. 7, which shows the experimental results of sample 4. There is a difference, however. Figure 7 shows an increase in luminescence intensity for various microwave powers and for every magnetic-field strength, while Fig. 14 shows a case such that luminescence intensity decreases with an influence of microwave absorption, for example, at 0 T with -1.6-, -5-, and -10-dB microwaves. The

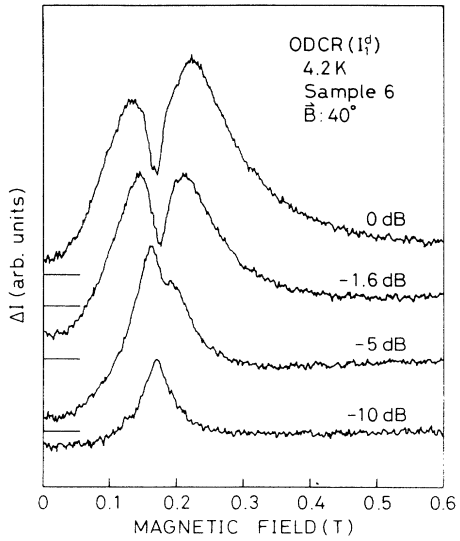

FIG. 14. ODCR traces obtained from the I_1^d line with various microwave powers. Because of the existence of twin boundaries, there is a component of photoluminescence intensity monotonically increasing with magnetic field that is especially remarkable for -5-dB microwaves.

difference originates in the fact that sample 6 is twinned. The process where electrons in the potential wells are captured into V_{Zn} states is not as simple as the one where bulk electrons are captured into V_{Zn} states as described in Sec. IV B, because electrons in the potential wells are located in the limited region of the sample and bulk electrons are populated in the whole region of the sample. The potential-well structure affects the capture rate. The anisotropy of the capture rate corresponding to the potential-well structure is shown in Fig. 15, where the dependence of ODCR upon magnetic-field direction is demonstrated. We have shown in Sec. IV C that the elec-

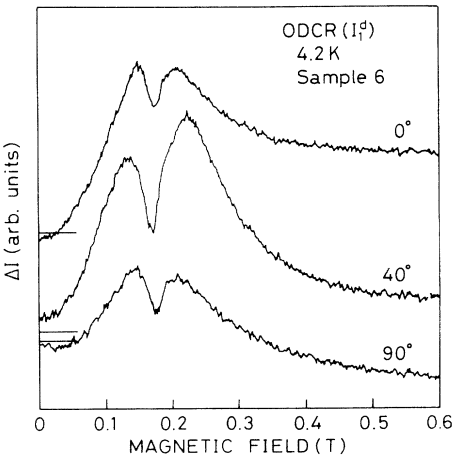

FIG. 15. Angular dependence of the ODCR trace obtained from the I_1^d line. The change in photoluminescence intensity at the high-magnetic-field side depends on the magnetic-field direction. The meaning of the angles is the same as in Fig. 9.

tron concentration in the potential wells is high in proportion with magnetic field when the magnetic-field component perpendicular to the plane of twin boundaries exists. It is probable that this fact is related to the experimental results in Fig. 15, because the increase in luminescence intensity at the high magnetic-field side is largest when the magnetic-field direction is perpendicular to the plane of twin boundaries.

In this section, we have shown, consistent with Sec. IV C, that the anisotropy of the potential-well structure affects the formation process of excitons bound to V_{Zn}. In other words, the formation rate of the bound excitons reflects the two dimensionality of electronic states in the potential wells.

V. SUMMARY AND CONCLUSIONS

We have studied decay kinetics of the photoexcited carriers in ZnSe by ODCR and TDCR. The most important conclusion in our ODCR study is that the characteristics of decay processes are determined by electron–polar-optical-phonon interaction. The evidences are (1) resonant formation of a free exciton following one LO-phonon emission, (2) a polaron effect in cyclotron resonance, and (3) electron capture cross section of deep A^+ centers dependent on electron energy. As to polaron cyclotron resonance, a peak shift of 4% has been observed in ODCR. Such a large peak shift is observed only in ODCR. Hence, the ODCR technique possibly opens a new avenue for polaron study. The second important conclusion is that the transition rate in the decay process is dependent on the kinetic situation of 2D electrons located in the twin-boundary region.

ACKNOWLEDGMENTS

We thank H. Nakata, K. Fujii, and H. Kobori for useful discussions and their help. We are grateful to S. Yoshimura for taking photographs of the samples. This work was partially supported by a Grant-in-Aid for Scientific Research on Priority Areas from the Ministry of Education, Science, and Culture. This work has been supported by the Subsidy for Special Equipment from the Ministry of Education, Science, and Culture. One of us (T.T.) has been supported by the Japan Society for the Promotion of Science.

---

*Present address: Advanced Research Laboratory, Hitachi Ltd., Hatoyama, Saitama 350-03, Japan.

†Present address: Ojiri 450-52, Hadano, Kanagawa 257, Japan.

[1]T. Ohyama, E. Otsuka, T. Yoshida, M. Isshiki, and K. Igaki, Jpn. J. Appl. Phys. **23**, L382 (1984).

[2]T. Ohyama, K. Sakakibara, E. Otsuka, M. Isshiki, and K. Igaki, Phys. Rev. B **37**, 6153 (1988).

[3]T. Ohyama, K. Sakakibara, E. Otsuka, M. Isshiki, and K. Masumoto, Jpn. J. Appl. Phys. **26**, L136 (1987).

[4]T. Ohyama, E. Otsuka, T. Yoshida, M. Isshiki, and K. Igaki, Surf. Sci. **170**, 491 (1986).

[5]J. L. Merz, H. Kukimoto, K. Nassau, and J. W. Shiever, Phys. Rev. B **6**, 545 (1972).

[6]P. J. Dean, D. C. Herbert, C. J. Werkhoven, B. J. Fitzpatrick, and R. N. Bhargava, Phys. Rev. B **23**, 4888 (1981).

[7]M. Isshiki, T. Kyotani, K. Masumoto, W. Uchida, and S. Suto, Phys. Rev. B **36**, 2568 (1987).

[8]T. Tomaru, T. Ohyama, and E. Otsuka, J. Phys. Soc. Jpn. **58**, 3718 (1989).

[9]T. Tomaru, T. Ohyama, and E. Otsuka, in *Proceedings of the Twentieth International Conference on the Physics of Semiconductors, Thessaloniki, 1990,* edited by E. M. Anastassakis and J. D. Joannopoulos (World Scientific, Singapore, 1990), p. 630.

[10]T. Tomaru, T. Ohyama, and E. Otsuka, Appl. Magn. Res. **2**, 379 (1991).

[11]T. Tomaru, T. Ohyama, and E. Otsuka, Phys. Rev. B **44**, 10 622 (1991).

[12]T. Tomaru, T. Ohyama, and E. Otsuka, Semicond. Sci. Technol. **7**, B256 (1992).

[13]T. Tomaru, T. Ohyama, and E. Otsuka, J. Phys. Soc. Jpn. **61**, 1798 (1992).

[14]K. Igaki and S. Sato, Jpn. J. Appl. Phys. **18**, 1965 (1979).

[15]X. Huang and K. Igaki, J. Cryst. Growth **78**, 24 (1986).

[16]S. Huang, Y. Nozue, and K. Igaki, Jpn. J. Appl. Phys. **22**, L420 (1983).

[17]I. J. Booth and C. F. Schwerdtfeger, Phys. Status Solidi B **130**, 749 (1985).

[18]G. E. Hite, D. T. F. Marple, M. Aven, and B. Segall, Phys. Rev. **156**, 850 (1967).

[19]K. K. Bajaj, Phys. Rev. **170**, 694 (1968).

[20]*Crystal and Solid State Physics,* edited by O. Madelung, Landolt-Börnstein, New Series, Group III, Vol. 17, Pt. b (Springer-Verlag, Berlin, 1982), p. 149.

[21]F. M. Peeters and J. T. Devreese, Phys. Rev. B **31**, 3689 (1985).

[22]T. D. Lee, F. E. Low, and D. Pines, Phys. Rev. **90**, 297 (1953).

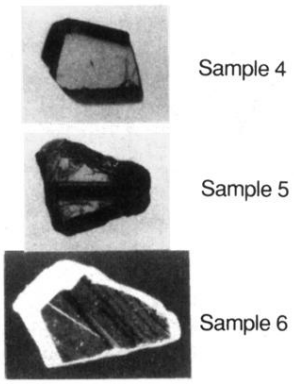

FIG. 1. Microscopic photographs of employed samples. Black stripes are twin boundaries. Photographed sample surface is a [110] crystallographic plane.